



DESIGN AND PERFORMANCE OF A LOW-COST SUBSONIC WIND TUNNEL

Alexander **BARON VON HOHENHAU**

Technical University of Cluj-Napoca

alex@edesign.co.uk

Keywords: Wind Tunnels, Turning Vanes, Diffusers, Flow Uniformity, Pressure Drop, Turbulence

Abstract: *This paper investigates the design and performance of a small-scale inexpensive wind tunnel, with a working cross-section of 305 by 305 mm and a top speed of 56 m/s, powered by an 18.5 kW centrifugal fan. The wind tunnel incorporates a diffuser, a contraction and various flow conditioners. Guidance on the construction and incorporation of each of these components is provided. Their performance was evaluated using a seven-hole probe and the results are compared to findings in literature. Particular attention is paid to flow uniformity and pressure changes. It is demonstrated that wire screens and honeycombs bring about clear improvements in flow quality, although their effect is eclipsed by the outstanding performance of a 4:1 contraction. It is demonstrated that the right design choices allow for the construction of a cost-effective wind tunnel capable of producing excellent flow uniformity with relatively low power requirements.*

1. INTRODUCTION

As part of a larger research effort relating to the design of expansion turning vanes, the author required a suitable aerodynamic testing environment. To this end, a small-scale wind tunnel was constructed. Excellent literature on the construction of wind tunnels already exists, namely publications by Barlow et al. [1] and de Almeida et al. [2]. However, these focus on mid to large-scale facilities and lack detailed flow contours of individual sections.

The open-circuit wind tunnel presented herein consists of five main components: A centrifugal fan, an expansion section, a set of simple turning vanes, a straight settling chamber, and a contraction. The following sections discuss the design and construction of the wind tunnel. This is followed by an analysis of the performance of various component configurations,

in regards to pressure drop and flow uniformity. Where advantageous, additional wire screens and honeycombs have been installed. The main requirements were to attain a minimum flow speed of 35 m/s and a turbulence intensity below 1% downstream of the contraction. The flow downstream of the numerous wind tunnel sections is characterised using a seven-hole probe.

2. WIND TUNNEL DESIGN AND CONSTRUCTION

The layout of the wind tunnel is shown in *Figure 1*, and the dimensions of the individual sections are summarised in Table 1. The sections were constructed from wood procured in the UK, where standard plywood sheets measure 2440 by 1220 mm. By making the typical cross-section of the tunnel 600 by 600 mm, and the length of most sections around 1220 mm, material wastage could be minimised. This reduced cost, while still facilitating a tunnel of adequate size. The rest of this section will discuss the various components of the wind tunnel in greater detail.

Table 1. Geometric characteristics of different wind tunnel components (all lengths are in metres)

Section	Inlet Width	Inlet Height	Outlet Width	Outlet Height	Centreline Length	Area Change (ratio)
Fan	NA	NA	0.394	0.631	NA	NA
Expansion	0.394	0.631	0.600	0.600	0.60	1.45
Curve	0.600	0.600	0.600	0.600	1.20	1.00
Straights	0.600	0.600	0.600	0.600	4.88	1.00
Nozzle	0.600	0.600	0.305	0.305	1.20	0.26

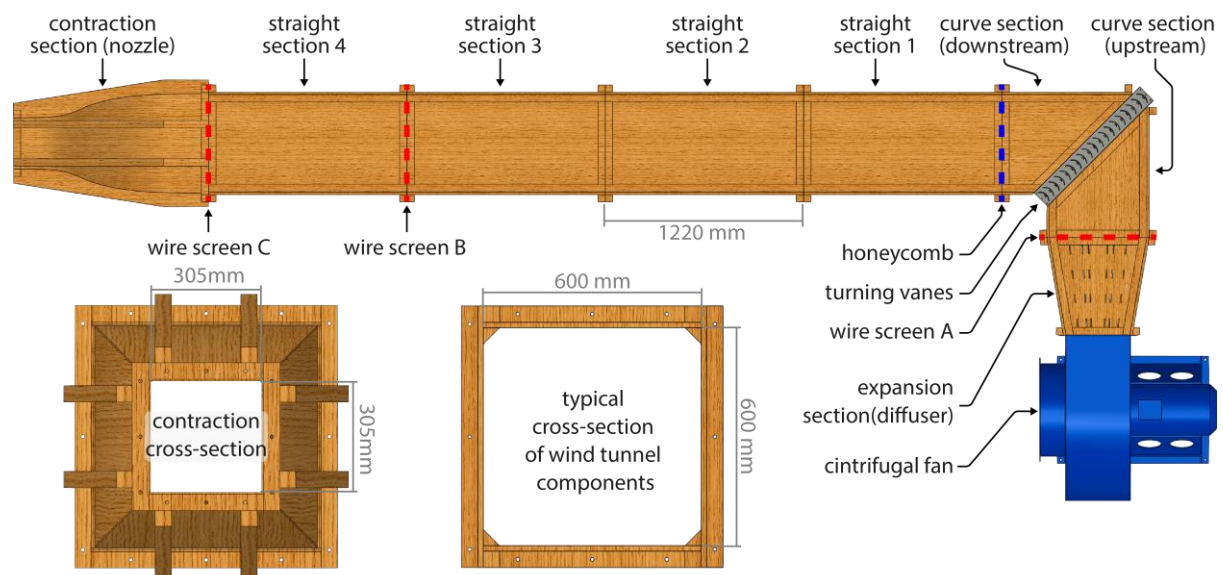


Figure 1. Birds-eye view of the wind tunnel and selected wind tunnel cross-sections. The honeycomb and wire screens are inside the tunnel and their locations are indicated by the dotted lines.

2.1. Constructing the Diffuser

The main purpose of the diffuser is to adapt the 631 by 394 mm cross-section of the fan to the 600 by 600 mm cross-section of the main wind tunnel segments. Due to space restriction, the diffuser length was limited to 598 mm, resulting in an expansion angle (2θ) of 19.48° . The diffuser size is normalised by dividing its length ($L = 598$ mm) by the inlet width ($D_1 = 394$) resulting in a ratio of 1.52. According to Smith and Kline, this places the diffuser at the upper limit of the region of no appreciable stall as shown in *Figure 2* [3]. The nearby region of large transitory stall is prone to flow unsteadiness, thereby negatively impacting the data quality of experiments conducted downstream.

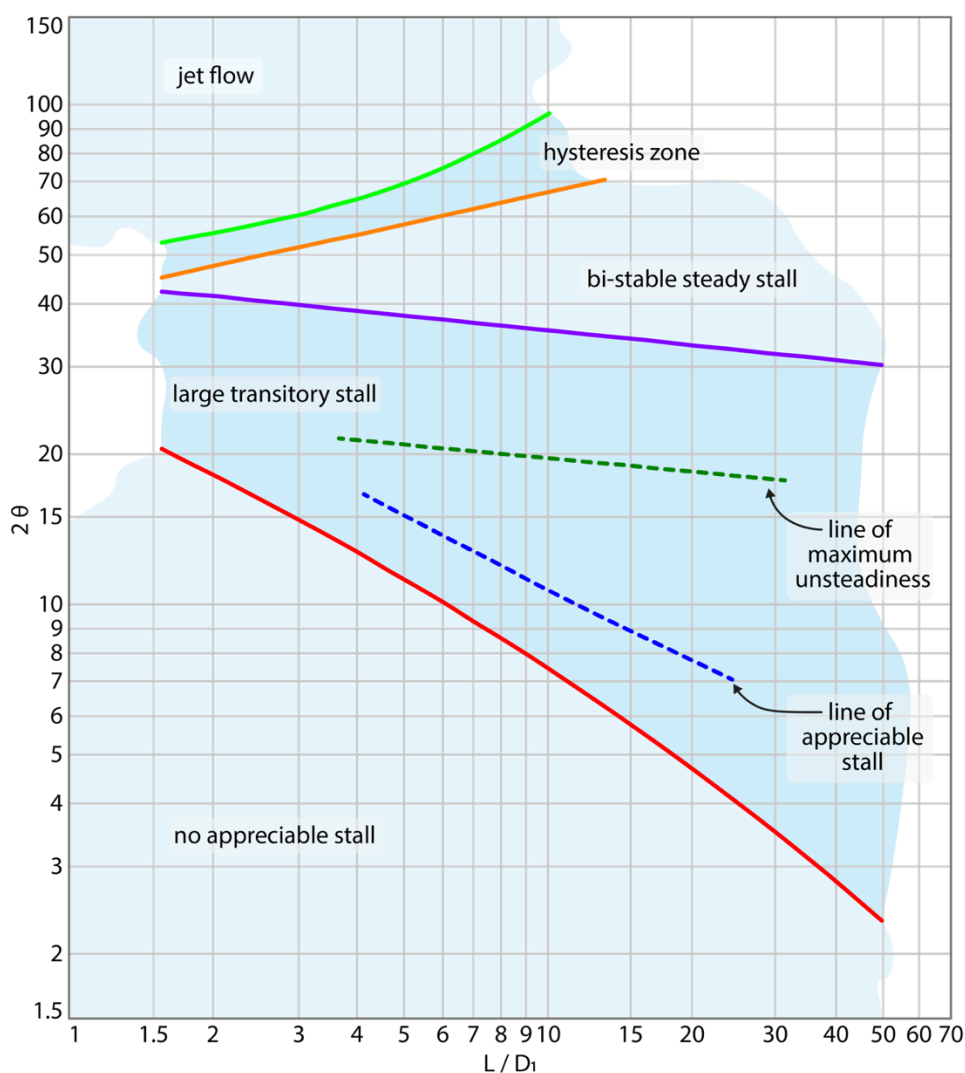


Figure 2. Stall regimes of diffusers with varying normalised diffuser sizes (L/D_1) and total expansion angles (2θ). Adapted from Smith & Kline [3].

Due to the proximity of the expansion geometry to the large transitory stall region, the diffuser was constructed in a manner that allowed for the insertion of dividing walls. This was achieved by placing slots into the floor and ceiling of the diffuser into which the dividers could

be inserted. For this project, the slots were created using a drill and a jig saw, although the author would recommend using a wood router instead, should one be available. The characteristics of the various diffuser configurations are summarised in Table 2.

Table 2: Geometric characteristics of different diffuser configurations

Dividers (QTY)	Inlet D_1 (m)	Outlet D_2 (m)	Length (m)	2θ ($^\circ$)	Length / D_1 (Ratio)
0	0.394	0.600	0.600	19.48	1.52
2	0.131	0.200	0.600	6.50	4.58
4	0.079	0.120	0.600	3.90	7.59

The configuration with four dividers is furthest from the region of large transitory stall, though both configurations using dividers are comfortably within the region of no appreciable stall. In addition to the various dividers, the diffuser can also be equipped with a wire screen, to further improve the stall characteristics and smooth the flow profile. Photographs of the different configurations are shown in *Figure 3*. As will be discussed in a subsequent section, the dividers were found to be disadvantageous to flow uniformity. Therefore, they were not used in the final version of the wind tunnel. The slots were sealed using silicone to reduce pressure losses through leakage and increased surface roughness.

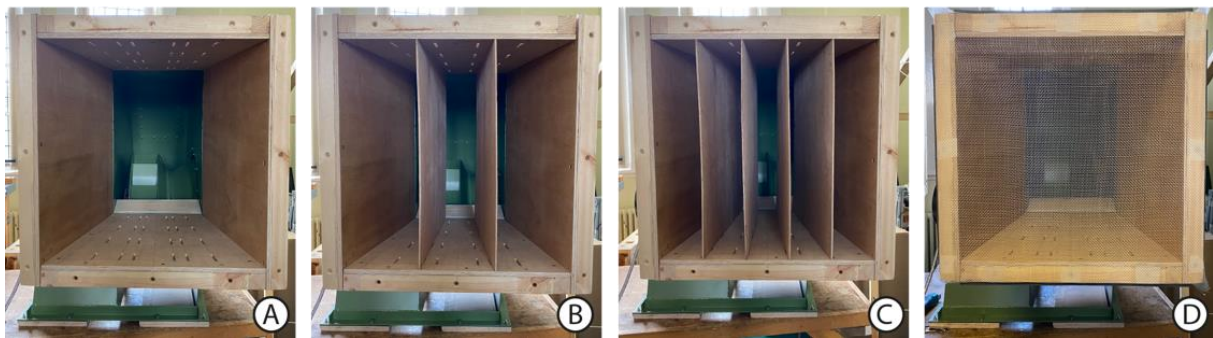


Figure 3. The diffuser with no dividers (A), two dividers (B), four dividers (C), and no dividers but with a wire screen (D). All configurations are shown attached to the fan.

2.2. Constructing the Curved Section

The aforementioned space restrictions also necessitated the use of a curve section within the tunnel. Regrettably, for this wind tunnel segment, there was an insufficient budget for extruding or pultruding complex aerofoil turning vanes. Printing these vanes was also unviable as the 600 mm channel height exceeded the size limit of the available 3D printer. Therefore, the best solution was to rely on the research of de Vega et al. and use circular flat plates that over-turn through 101° [4].

The vanes were manufactured by trimming semi-circular PVC gutter pipe with a thickness of 2 mm. Sharp edges were deburred and the leading edge was sanded smooth. To ensure the correct vane position and spacing, two mild steel plates were laser cut and folded with slots for the vanes and holes for mounting the assembly to the wind tunnel. Correct spacing between the plates was ensured by using M6 threaded bars and nylon-insert nuts. The vanes were secured in their slots using standard silicone. The completed setup is shown in *Figure 4*.



Figure 4. Internal of the curve (A), birds-eye view of the curve (B) and seal between the outer vane and the wind tunnel sections (C).

Unfortunately, this method of constructing the vane section leaves four gaps between the outermost vanes and the wind tunnel. It is required to seal these gaps to prevent the high-pressure flows in the wind tunnel from jetting out at this segment. Failure to do so would lead to energy losses and ultimately a lower maximum flow rate. The gaps were initially sealed using standard masking tape. While this was not an issue at lower speeds, the seal at the outer turning vane tended to rupture when flow velocities and pressures were higher. After several iterations of using more and different tape, it was decided that a sturdier solution was needed. The tape seals were replaced with smooth waterproof plastic fabric, which was rigidly clamped against the wood (see the right of *Figure 4*). No further sealing issues were observed thereafter.

2.3. Constructing the Straight Sections

The straight tunnel sections are by far the easiest to construct, but they should still be assembled with care as they make up the majority of the wind tunnel and are intended to contribute to a smooth velocity profile at the test section. The sections were constructed in a manner that allowed for the addition of small corner chamfers. These chamfers are said to reduce the level of secondary flow, thereby increasing flow uniformity [4]. The chamfers were cut from lengths of 45 by 45 mm dressed wood using a table saw with a blade angle of 45°. Due to blade kerf, the resulting chamfers are approximately 43 by 43 mm wide. *Figure 5* shows the various stages of construction of the straight sections.

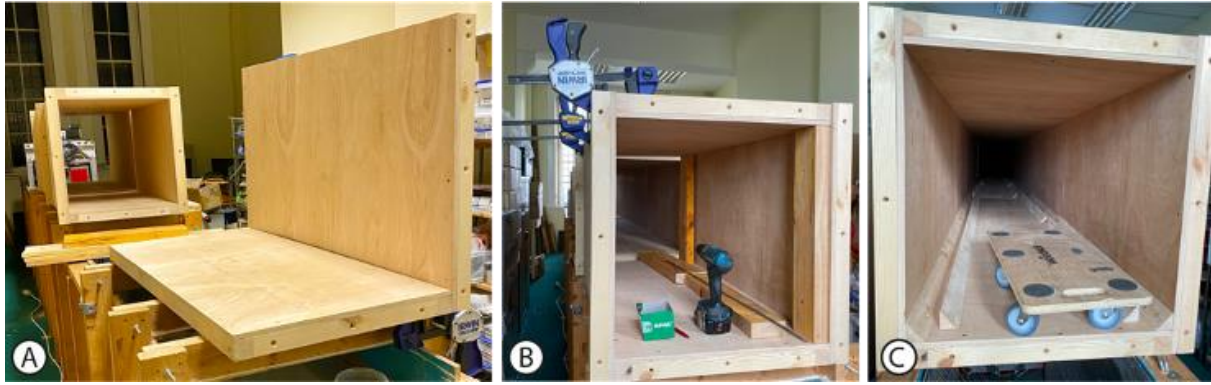


Figure 5. Initial construction of a straight section (A), top panel installation using spacers (B), and chamfer installation with the bottom pieces already fixed in place (C).

The main difficulty in constructing the straight section (and most other sections) lies in the need to accurately assemble the wood. The bottom and top panels were delivered slightly oversized. They were subsequently trimmed to 600 mm using a band saw to give a precise channel width. The panels were assembled using wooden spacers to ensure accurate channel height. Great care was taken to ensure that the flanges on each component, particularly the bolt holes would line up with the other sections. This ensured easy assembly, smooth transitions on the inside of the tunnel, and cross-compatibility between the sections (i.e., it did not matter in which order the straight sections were assembled or how many were actually used). Accurate hole placement was aided through the use of a 3D-printed drilling jig, which indicated the right distance to the end and the correct positioning on the centreline of the timber pieces.

2.4. Constructing the Contraction

Out of all the wind tunnel segments, the construction of the contraction was by far the most challenging. The first problem is posed by the shape. The curve is based on the pressure gradient optimisation conducted by Alfredsson and Sahlin [5]. The underlying function is shown below. Here, L is the contraction total length, x is the variable distance along the contraction, and A , B , C , and D are constants:

$$f = A \left(\sinh \left(B \frac{x}{L} \right) - B \frac{x}{L} \right) \quad \text{when } \frac{x}{L} \leq 0.7 \quad (1)$$

$$f = 1.0 - C \left(\sinh \left(D \left(1 - \frac{x}{L} \right) \right) - D \left(1 - \frac{x}{L} \right) \right) \quad \text{when } \frac{x}{L} > 0.7 \quad (2)$$

$$A = 0.205819 \quad B = 3.52918 \quad C = 0.08819 \quad D = 8.23523$$

The actual shape of the contraction is determined using the following equation, where w_{local} is the local width, w_{max} is the maximum width, and R_c is the contraction ratio:

$$w_{local} = \pm w_{min} \left(\frac{R_c}{2} (1 - f) + \frac{1}{2} f \right) \quad (3)$$

A diffuser with a length of 1200 mm, an inlet width of 600 mm, and an outlet width of 305 mm has a contraction ratio of approximately 2:1. Graphing the equations outlined herein, the diffuser curves obtained are shown in *Figure 6*.

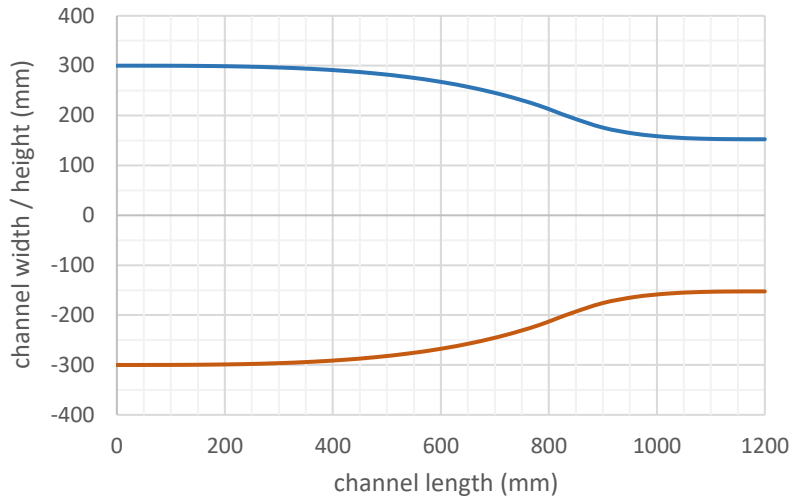


Figure 6. Contraction curves used to define the shoe of the contraction

Equipped with the correct curve equations, the diffuser can be modelled in 3D CAD software, in this case, SolidWorks. The exact dimensions are chosen so that the curve length of the diffuser is 1220 mm, thereby minimising material wastage. The inlet is 600 x 600 mm, while the outlet is 305 x 305 mm. After establishing a shape, the means of constructing the diffuser had to be found. The author thought it would be best to construct the walls of plywood and supporting ribs of dressed timber, as shown in *Figure 7*.

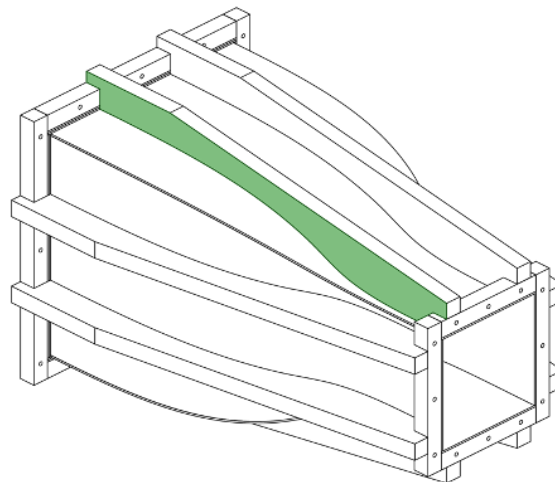


Figure 7: 3D Model of contraction made from 5mm plywood walls and 120 x 45mm timber ribs. The ribs were carefully shaped to provide the correct curvature.

The 3D model of the contraction was turned into a series of manufacturing drawings. A simplified version of one of these drawings is shown in *Figure 8*.

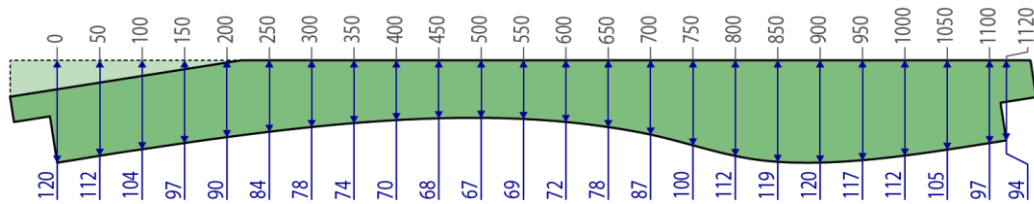


Figure 8. Dimensions (in mm) of the rib curve used for the contraction section. The 0 ordinate marks the beginning of the curve.

The ribs were cut using a band saw and precisely finished using a linisher. Due to the intricate curves of the contraction, a substantial amount of time had to be spent on marking and cutting the wood. The curved walls posed numerous further challenges. They were made from 5mm plywood, which proved difficult to bend sufficiently to fit the ribs. To increase malleability, the plywood was soaked in water for several hours. However, even after this procedure, a lot of pressure was required to force them into the correct shape.

For future endeavours of this kind, the author would recommend using 3mm plywood instead, as it should be more flexible, yet still offer enough strength to cope with the forces exerted by the flow. To cut the plywood to the correct shape, a projection tool within SolidWorks was used to map the curved walls onto a flat surface. Unfortunately, this projection was slightly inaccurate, which led to gaps in the corners, as shown in *Figure 9*.

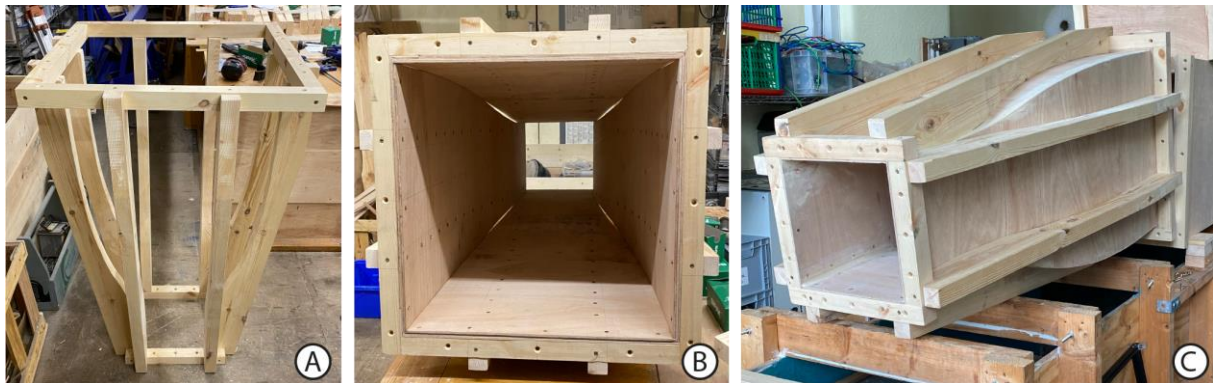


Figure 9. Contraction support structure without walls (A), the interior of contraction with corner gaps (B), and final contraction with gaps sealed using wood filler (C).

3. RESULTS AND DISCUSSION

The main performance criteria for the wind tunnel section are flow uniformity and pressure loss. While there are numerous measures of flow uniformity, this report will use the

coefficient of variation (CV). It is calculated by dividing the standard deviation (σ) of a data set by its average (x_{avg}), as shown in equation (4), where, x_i represents individual data points.

$$CV = \frac{\sigma}{x_{avg}} = \frac{1}{x_{avg}} \sqrt{\frac{1}{n} \sum_{i=1}^n (x_i - x_{avg})^2} \quad (4)$$

Pressure loss is best represented through the non-dimensional loss factor K as shown in equation (5). The loss factor is simply the ratio of the local pressure loss and the dynamic pressure in the flow.

$$\Delta p = \frac{1}{2} K \rho u^2 \quad (5)$$

With many flow conditioners, a higher loss factor is often associated with increased flow uniformity. This is particularly true for wire screens and honeycombs. A good compromise has to be found to ensure that flow conditioners provide sufficiently uniform flow without incurring excessive pressure losses, as these are linearly correlated to power consumption. Unless otherwise indicated, the experiments outlined henceforth were run at a constant fan speed of 2700 RPM, requiring 12.8 kW of power.

The flow was measured using an individually calibrated seven-hole probe and a digital pressure scanner. The latter was equipped with three sets of eight channels, capable of measuring pressure ranges of 160, 1000 and 4000 Pa. The nominal accuracy of each set was $\pm 0.25\%$ of its range, which equates to 0.4, 2.5 and 10 Pa respectively. For a majority of the experiments, the seven-hole probe was connected to the 4000 Pa channels. Both the probe and the scanner were supplied by Surrey Sensors. The outlet of the fan was surveyed in a 13 by 21 point grid, while all the square cross-sections are surveyed using a grid of 21 by 21 points. Each grid point was sampled for 5 seconds and a frequency of 100 Hz. The graphs herein were generated from approximately four million data points. This data set is too large to be included herein but is available from the author upon request. For velocity contours, the individual velocity measurements (u) have been normalised using the local average velocity (u_{avg}).

3.1. Flow conditions at the fan outlet

The flow fan was purchased from Greenmount Fans in England. It was immediately apparent that the volute tongue, was a simple folded piece of sheet metal, creating a sharp step towards the exit of the fan (see *Figure 10*). This design certainly leads to flow separation and flow recirculation in the area immediately downstream of the step.

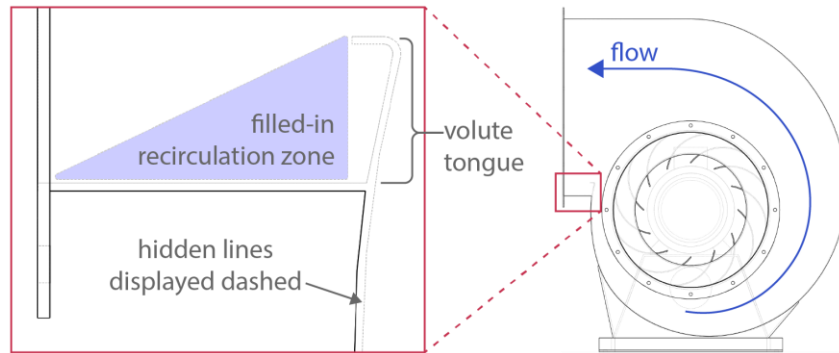


Figure 10: Side section view of the fan with a detailed view showing the wedge's location

Without fundamentally changing the fan design, the contours presented by Wang et al. suggested that filling this zone with a wooden edge would help to improve the quality of the flow [6]. Figure 11 shows the fan before and after the installation of this wedge. Flow measurements were taken before and after the installation.

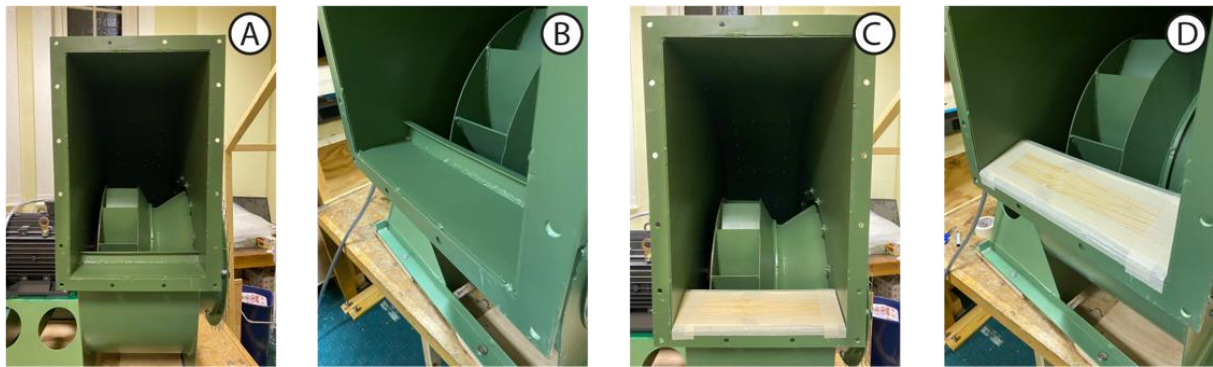


Figure 11: Flow fan without modifications (A and B) & with a wedge installed at the exit (C and D).

From the velocity profiles shown in figure 12, it is clear that the flow is highly three-dimensional. The magnitude of the secondary flow (indicated by arrows) is up to 60% as large as the primary flow (indicated by the colours in the contour).

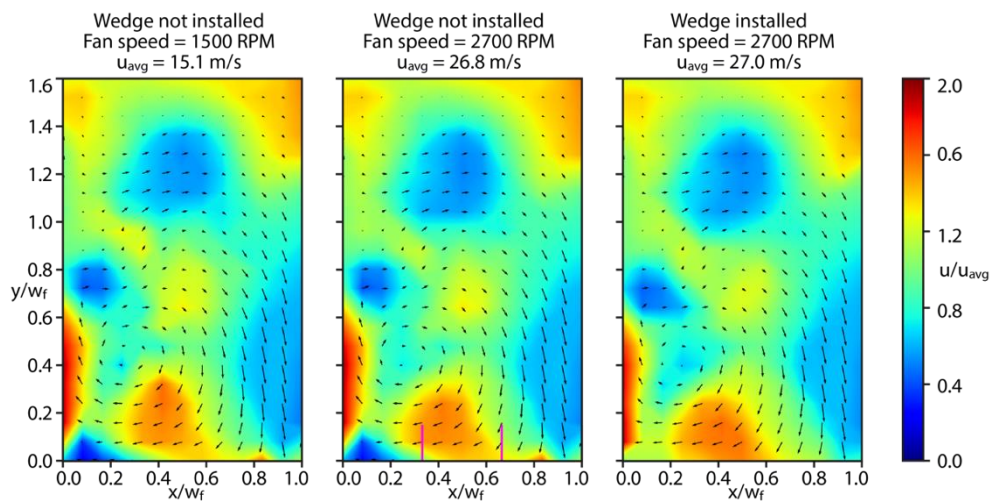


Figure 12. Velocity contours at the fan outlet, before and after the installation of the wedge.

The rotation of the blades and the fan geometry form a strong clockwise vortex, which is present in all trials. Varying the RPM across normal testing ranges has little effect on the velocity distribution. The installation of the wooden wedge facilitates the movement of flow toward the bottom-left corner. Additionally, the general flow uniformity is increased as the coefficient of variance is decreased from 0.235 to 0.230.

3.2. Performance of the Diffuser

It is generally favourable to have diffusers with lower expansion angles. However, the diffuser for this wind tunnel had to be fairly short, resulting in a relatively large expansion angle. To lower the expansion angle, dividing walls could be installed within the diffuser. *Figure 13* compares using zero, two and four dividing walls. Due to the highly three-dimensional nature of the flow, the dividing walls are disadvantageous. Instead of aiding the expansion, they isolate areas of flow. This means that high and low-velocity flows cannot mix, thereby reducing flow uniformity. The coefficient of variation with zero, two and four dividing walls is 0.276, 0.365, and 0.334 respectively.

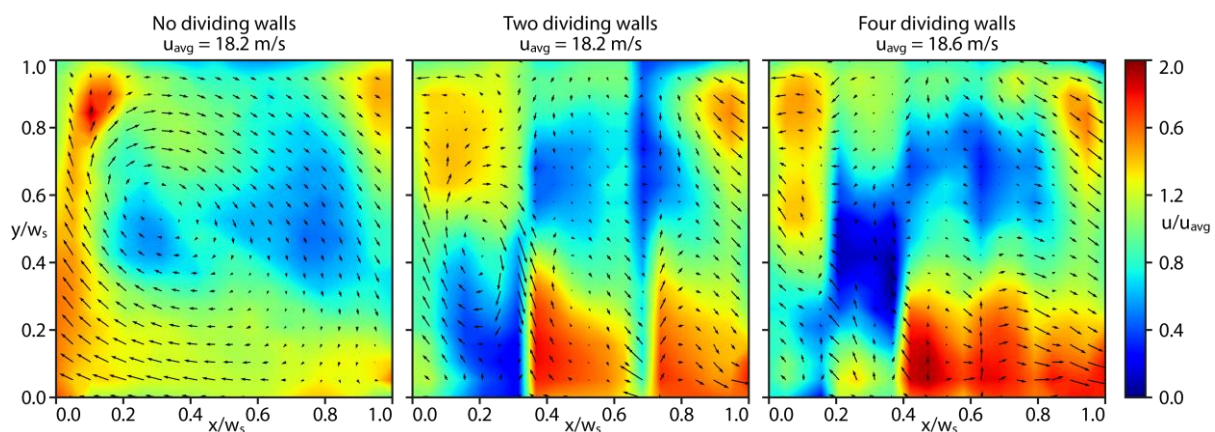


Figure 13: Velocity contours at the expansion outlet with a varying number of dividing walls

Instead of incorporating dividing walls, the diffuser can also be fitted with a wire screen. Unfortunately, as the flow passes the wire screen, small jets are created by the individual holes in the screen. These jets can disturb the velocity probe measurements, as shown in the centre of *Figure 14*. To avoid such disturbances, the measurements can be taken further downstream, where the jets have dissipated, as shown on the right of *Figure 14*. Here, it is apparent that the wire screen smoothed the flow contour and the CV is reduced from 0.262 to 0.159.

Conservatively evaluating the pressure losses at the wire screen downstream of the expansion, the loss factor K is found to be 1.193 ± 0.090 . This is slightly below the value of 1.333 predicted based on the works of Wu et al. [8].

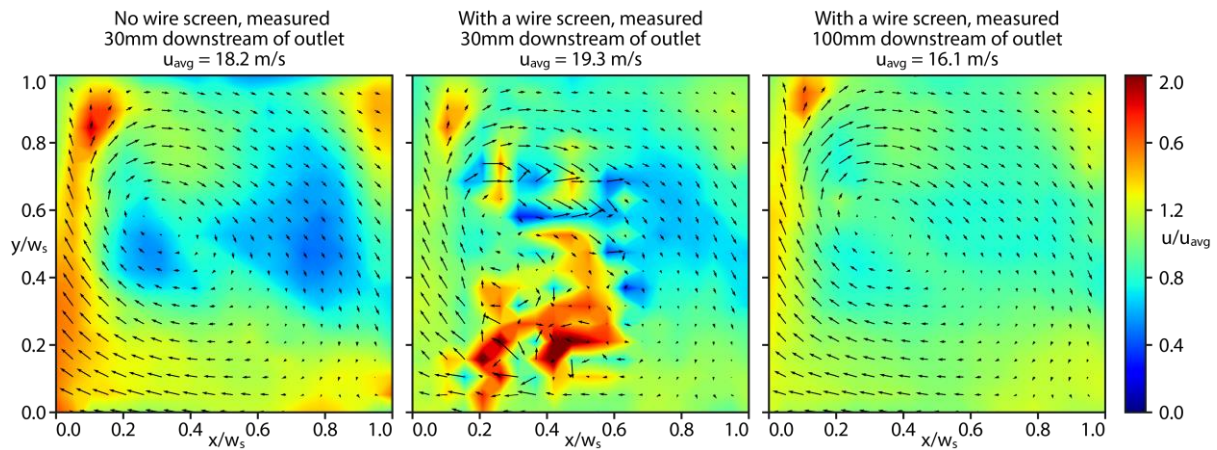


Figure 14: Velocity contours of the expansion before and after installing a wire screen

Based on flow rate measurements taken at the wind tunnel outlet, the dynamic pressures can be calculated for each wind tunnel section. This allows for an estimation of the total pressure drop through the diffuser. Based on the inlet velocity, the diffuser has a loss factor K of 0.410 ± 0.019 .

In this location, some of the error can be attributed to regular vortices caused by the centrifugal blades of the fan and the random noise within the pressure measurements themselves. The theoretical loss factor prediction based on a publication by Eckert et al. is merely 0.05 [7]. Despite the loss factor in this section being substantially higher than the literature-based prediction, it is still small enough to reach satisfactory speeds in the wind tunnel.

3.3. Performance of the Turning Vanes and Honeycomb

Due to the structure of the curved section containing the turning vanes, the velocity could not be measured in the proximity of the vane cascade. Instead, the velocity was sampled 230 to 300 mm downstream of the inner vane and 830 to 900 mm downstream of the outer vane, as shown in *Figure 15*.

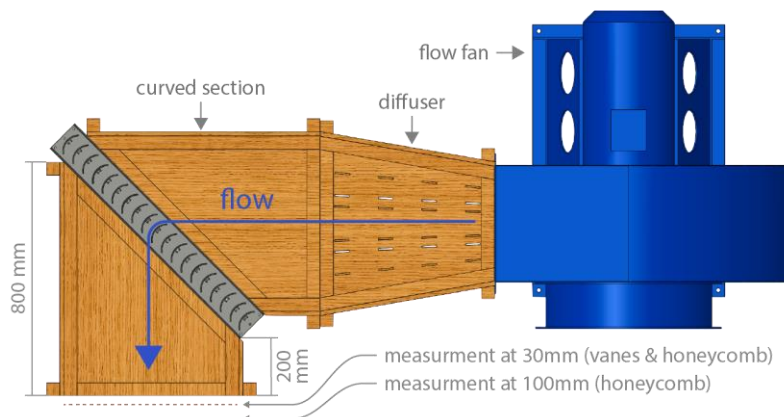


Figure 15. Birds-eye view of measurement planes used to generate the primary velocity contours shown in Figure 16

Experiments were carried out with and without the honeycomb and the resulting primary velocity contours are shown in *Figure 16*. Once again, the central contour reveals measurements that were taken too close to the flow conditioner. Where the probe aligns with a honeycomb tube it reads unreasonably high velocity and where it aligns with a tube wall it returns excessively low velocity. Thus, the resulting data seem somewhat nonsensical. As with the wire screen, this can be mitigated by taking measurements further downstream.

Upon inspecting the size and direction of the velocity vectors it becomes apparent that the secondary flow is almost entirely eliminated. Unfortunately, the honeycomb also seems to slightly increase the size of the boundary layer, as indicated by the areas of slow flow around the perimeter of the right-most contour. This means that the coefficient of variance is increased slightly from 0.125 to 0.152. Despite this increase, the honeycomb was kept in place for most further experiments, as it was deemed worthy to sacrifice a little flow uniformity for the elimination of secondary flow.

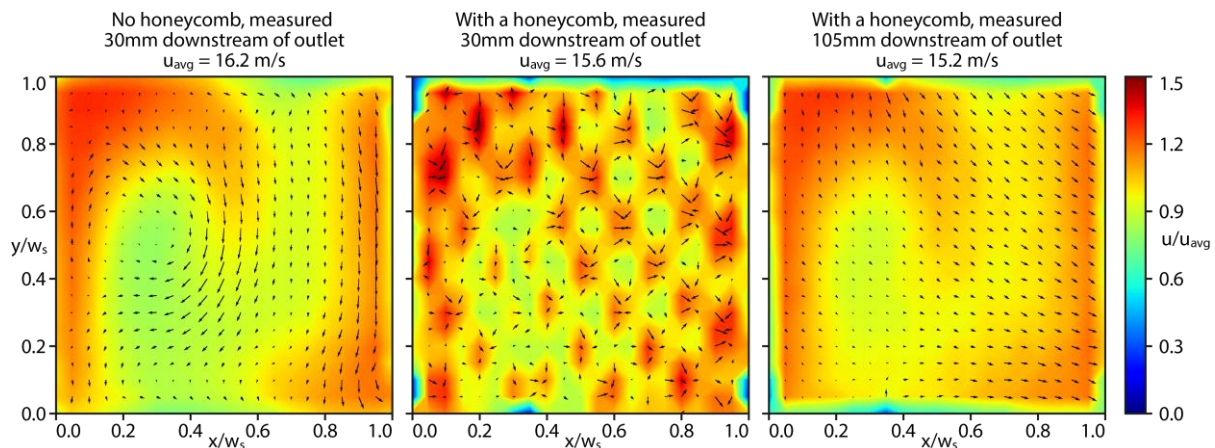


Figure 16. Velocity contours before and after installing a honeycomb downstream of the vanes

It was found that the vanes have a loss factor K of 0.258 ± 0.028 , which is roughly in line with the 0.300 predicted by Vega et al. [4]. The honeycomb has a loss factor K of 0.813 ± 0.475 which is significantly higher than the literary value of 0.380, which is based on the works of Innocentini et al. [9]. The higher standard deviation is caused by the loss factor of the honeycomb not scaling with the square of the velocity. While the loss factor is around 1.96 at 1.27 m/s, it drops to 0.42 at 12.71 m/s, which is considerably closer to the value suggested in literature. As power requirements only become an issue at higher flow velocities, this discrepancy will not prevent reaching the desired wind tunnel speeds.

3.4. Effect of adding corner chamfers

The installation of the corner chamfers slightly lowered the CV in the straight sections from 0.133 to 0.127. However, this corresponds to a mere 0.07m/s reduction in the standard

deviation, which is negligible when compared to the average primary flow velocity of 16 m/s. Vega et al. suggest that the chamfers would increase the CV by reducing secondary flow, but this cannot be independently verified here [4]. Potentially the corner chamfers are too small, as their base size is only 43 mm compared to the 600 mm channel width. Nevertheless, the chamfers clearly do not have any substantial negative impacts on the flow either. Therefore, they were left in place for the majority of further experiments.

3.5. Performance of the Contraction

Measuring the flow downstream of the contraction is challenging, as the boundary layer in this section is very thin and the flow velocity is rapid. Without any flow conditioners installed, the wind tunnel can achieve speeds up to 56 m/s, which corresponds to 203 km/h or 126 mph. For reference, the highest-level wind speed (“hurricane force”) on the Beaufort scale is 12, measuring a meagre 33 m/s (118 km/h or 73 mph).

When considering these speeds, it is clear that the rate of change of velocity in the boundary layer is very high. Consequently, the measurements are very sensitive to the location of the seven-hole probe. Even deviations of a single millimetre can change the readings substantially. Great care was taken to set the probe’s positions correctly, but a tolerance of ± 1 mm is to be expected.

Table 3. Overview of various coefficients of variance for different flow conditioner configurations

	before contraction (all points)	after contraction (all points)	after contraction (no edge points)
CV (no conditioners)	0.133	0.0442	0.00410
CV (all conditioners)	0.103	0.0499	0.00516

As shown in Table 3, the wire screens and honeycomb reduce the coefficient of variance upstream of the contraction by 23% (from 0.133 to 0.103). Interestingly, this effect does not translate downstream of the contraction. Before installing the flow conditioners, the contraction reduces the CV by 77% (from 0.133 to 0.0442), but only by 52% (from 0.103 to 0.0499) thereafter. Even when discounting the measurements on the circumference of the grid, the most sensitive to the positioning of the probe, the CV is still lower in the flow without flow conditioners.

The most probable explanation is that the measurement technique has reached an accuracy limit, as the difference between a CV of 0.0442 and 0.0499 is merely 0.0077. This approximately corresponds to a difference in the standard deviation of 0.0302 m/s. Here it is worth noting that the sensor card used for this set of trials had a measurement range of 4000 Pa and a tolerance of $\pm 0.25\%$ (or 10 Pa). The pressure tolerance can be expressed in terms of

velocity by using equation (6), where P is pressure, ρ is the fluid density and u is the fluid velocity:

$$u = \sqrt{2 P / \rho} \tag{6}$$

The 10 Pa tolerance is equivalent to a speed of roughly 4 m/s for a single measurement. However, a lower standard error is produced by sampling the pressure at a rate of 100 Hz over several seconds at each point. Thus, the average standard deviation across time after all flow conditioners have been installed is 0.219 m/s. This is not to be confused with the standard deviation of the flow field across space, which is the deviation of the time-averaged velocities between measurement points and equates to 0.232 m/s. Both values significantly exceed the 0.0302 m/s increase in deviation encountered after installing the flow conditioners.

In summary, the contraction works exceptionally well. As shown in *Figure 17*, it produces a very smooth velocity contour, regardless of the use of flow conditioners. Should it not be possible to incorporate a contraction into a testing facility, wire screens can be used to increase flow uniformity by reducing peaks in the velocity profile. Honeycombs can be used to reduce the magnitude of the secondary flows, an improvement visible even downstream of the contraction. Nevertheless, the impact of these types of conditioners is far inferior to that of the 4:1 contraction.

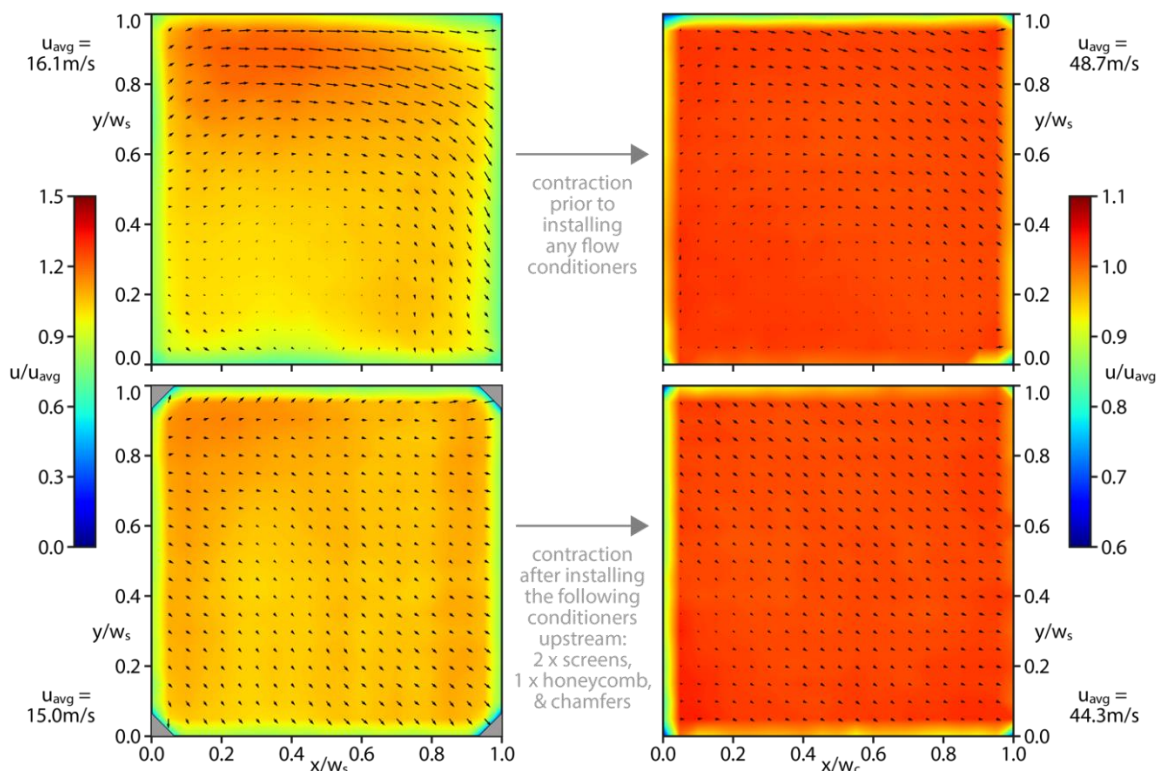


Figure 17. Comparison of velocity contours before (left) and after (right) passing through the flow contraction, with (top) and without (bottom) flow conditioners.

The experiments that have been described over the previous pages have been essential in validating that an adequate environment, for testing expansion turning vanes, has been provided. As can be seen from *Figure 17*, the contours have a slight secondary flow to the right. This is likely to do with the location of the flow fan, encouraging the flow to take the path of least resistance when leaving the tunnel, which coincidentally is towards the right.

For a majority of the flow field downstream of the contraction, the magnitude of this secondary velocity is approximately 1.2 m/s. This is equivalent to merely 2.5% of the primary velocity magnitude and, therefore, should have a negligible impact on the flow results and analysis. The turbulence intensity downstream of the contraction is 0.5% and is comfortably below the required upper limit of 1%. As shown in the contours, even with the flow conditioners installed, the wind tunnel is more than capable of reaching an average flow speed of 35 m/s downstream of the contraction. As such, all flow quality requirements have been met.

4. SUMMARY OF PRESSURE DROP PERFORMANCE

The theoretical loss factor for the straight section has been calculated using the Darcy-Weisbach equation, based on the friction factor f . Note that this factor is often determined using the Moody Chart or iterative calculations [10]. The author has found it useful to use the Sonnad-Goudar correlation instead, a non-iterative equivalent to the Colebrook-White equation [11]. Using this theoretical approach, the loss factor is predicted to be 0.017. This is in stark contrast to the experimental loss coefficient of 0.102 (see *Figure 18*).

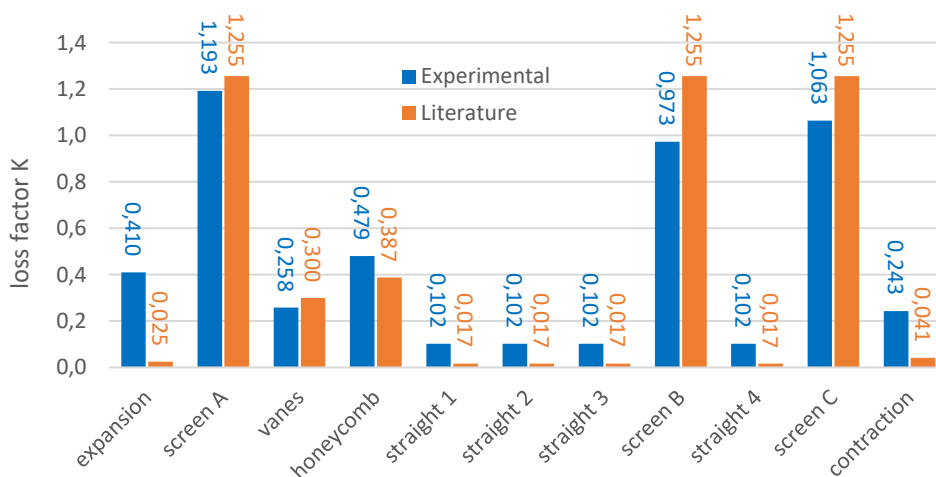


Figure 18. Theoretical versus measured pressure drops in the wind tunnel.

The difference is likely caused by the seam between the sections. While great care was taken to make the transitions as smooth as possible, small mismatches remain. However, the loss factor of the straight section becomes negligible when compared to the loss factor of the

screens. The screens clearly lead to the largest pressure drop in the system and the experimental loss being smaller than the prediction is to be taken as a clear positive.

5. CONCLUDING REMARKS

The flow characterisations demonstrate that it is possible to construct a small-scale wind tunnel with a relatively modest budget without having to sacrifice flow quality. However, building such a facility in-house is time intensive. It took approximately four months of full-time work to carry out the necessary steps (design, quotation, installation, commissioning, etc.) and another six weeks to complete the characterisation. Other key findings are summarised below:

- Conditioning the flow immediately downstream of a fan should be done with care. The flow in this area tends to be highly three-dimensional. Conditioners that segment the flow, such as dividing walls or coarse honeycombs, have the potential to decrease flow uniformity.
- Should it not be possible to include a contraction, it is possible to achieve significant improvements in the flow using honeycombs and wire screens. The former help to suppress secondary flows while the latter increases flow uniformity.
- A good contraction is key to ensuring high flow quality in the test section. The geometry used in this particular wind tunnel works so well, that it almost completely overshadows the effect of the wire screens and honeycomb.
- When incorporating wire screens, the designer should expect these flow conditioners to require a significant portion of the available power. In this system, more than half of the total pressure losses can be attributed to the three screens.

REFERENCES

- [1] J. B. Barlow, §W. H. Rae and A. Pope, *Low-Speed Wind Tunnel Testing*, New York: John Wiley & Sons Inc., 1999.
- [2] O. de Almeida, F. C. de Miranda, O. F. Neto and F. G. Saad, *Low Subsonic Wind Tunnel-Design and Construction*, Journal of Aerospace Technology and Management, vol. 10, 2018.
- [3] C. R. Smith and S. J. Kline, *An Experimental Investigation of the Transitory Stall Regime in Two-Dimensional Diffusers*, Journal of Fluids Engineering, pp. 11-15, 1974.
- [4] L. L. de Vega, F. J. M. Fernández and P. M. Botas, *Optimisation of a Low-Speed Wind Tunnel - Analysis and Redesign of Corner Vanes*, pp. 1-152, 2014.

- [5] B. Lindgren and A. V. Johansson, *Design and Evaluation of a Low-Speed Wind-Tunnel with Expanding Corners*, Royal Institute of Technology, Stockholm, 2002.
- [6] K. Wang, J. Yaping and C. Zhang, *Aerodynamic optimization of forward-curved blade centrifugal fan characterized by inclining bionic volute tongue*, *Structural and Multidisciplinary Optimization*, vol. 63, p. 2493–2507, 2021.
- [7] W. T. Eckert, K. W. Mort and J. Jeau, *Aerodynamic Design Guidelines and Computer Program for Estimation of Subsonic Wind Tunnel Performance*, National Aeronautics and Space Administration (NASA), Washington DC., 1976.
- [8] W. T. Wu, J. F. Liu and W. H. Hsieh, *Measurement and correlation of hydraulic resistance of flow through woven metal screens*, *International Journal of Heat and Mass Transfer*, vol. 48, no. 14, pp. 3008-3017, 2005.
- [9] M. D. M. Innocentini, V. R. Salvini, A. Macedo and V. C. Pandolfelli, *Prediction of Ceramic Foams Permeability Using Ergun's Equation*, *Materials Research*, vol. 2, no. 4, pp. 283-289, 1999.
- [10] L. F. Moody, *Friction factor for pipe flow*, *Transactions of the A.S.M.E.*, pp. 671-684, 1944.
- [11] J. R. Sonnad and C. T. Goudar, *Turbulent Flow Friction Factor Calculation Using a Mathematically Exact Alternative to the Colebrook–White Equation*, *Journal of Hydraulic Engineering*, pp. 863-867, 2006.
- [12] *Employee earnings in the UK: 2020*, Office for National Statistics, London, 2021.